RSC Advances

ROYAL SOCIETY OF CHEMISTRY

www.rsc.org/advances

A table of contents entry

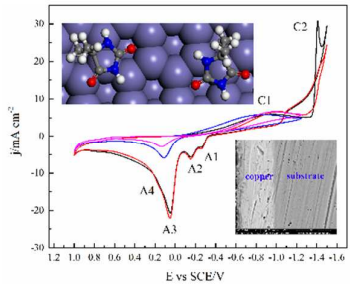

Electrochemical methods, including cyclic voltammetry, chronoamperometry, and chronopotentiometry, combined with molecular dynamic simulation are used to study the electrodeposition mechanism.

Electrodeposit Copper from alkaline cyanide-free baths containing 5, 5'- dimethylhydantoin and citrate as complex agents

Jie Zhang, Anmin Liu, Xuefeng Ren, Jinqiu Zhang, Peixia Yang and Maozhong An[1]
State Key Laboratory of Urban Water Resource and Environment, School of Chemical Engineering and Technology, Harbin Institute of Technology, Harbin 150001, China

Abstract:

An alkaline cyanide-free bath containing 5, 5'- dimethylhydantoin (DMH) and citrate as the complex agents was investigated and developed for copper electrodeposition on carbon steel substrate. The cathodic electrodeposition process was studied by electrochemical measurements including cyclic voltammetry, chronoamperometry, chronopotentiometry, and cathodic polarization on the platinum and glass carbon disk electrodes. Copper layers were characterized with SEM for surface morphology, XRD for crystal structure, and three qualitative methods for adhesion evaluation. On the basis of the analysis of cyclic voltammetry with various switch potentials, the discharge processes in the solutions with only DMH, only citrate, and both as the complex agents have the typical two steps. The discharge processes of both copper-DMH and copper-citrate complexes are irreversible according to the cyclic voltammetry with various scan rates, which is combined with sample current voltammetry to get the kinetic parameters. Diffusion coefficients were calculated from the chronoamperometry according to Contrell equation. The

[1] Corresponding author at: State Key Laboratory of Urban Water Resource and Environment, School of Chemical Engineering and Technology, Harbin Institute of Technology, No. 92 Xidazhijie Street, Nangang District, Harbin, 150001, China. Tel.: +86-451-86418616. Fax: +86-451-86418616.
E-mail address: mzan@hit.edu.cn (Maozhong An)

nucleation and crystal growth processes on the glass carbon electrode in these three solutions show an agreement with the progressive nucleation process of SH models. Molecular dynamic simulation reveals that the plane of the heterocycle of all the four DMH molecules simulated are parallel to the Fe (111) surface and the interaction energy between various molecules and Cu (111) as well as Fe (111) surface were compared. DMH molecules adsorbed on the carbon steel electrode desorb at the initial stage of electrodeposition, which was determined by potential *vs*. time curves. The concentration of DMH and K_2CO_3 as well as the value of pH have a crucial effect on the surface morphology, the preferable crystal orientation, and the adhesion of the copper layers electroplated on carbon steel substrate. The electrodeposited copper layers had good adhesion with the carbon steel substrate and the average grain size is about 30 nm. The optimum bath is composed of 0.1 M $CuSO_4$, 0.2 M DMH, 0.3 M citrate, and 0.3 M K_2CO_3 at pH 9 ~10.5 and 50℃.

Keywords: Copper electrodeposition, Alkaline cyanide-free, 5, 5'-dimethylhydantoin, Sample current voltammetry, Cyclic voltammetry

1 Introduction

Alkaline cyanide baths are still used to electroplate copper that has many applications for the metal-finishing industry [1]. In recent decades many different alternative electrolytes, such as solutions containing amine–ammonia, chloride, citrate, EDTA, glycerolate, phosphate, pyrophosphate, tartrate, and triethanolamine [1], sorbitol [2, 3], tartrate [4], and glycine [5, 6], have been proposed and studied around the world to replace cyanide baths for its environment issues. Owing to economic, chemical, environmental or some other limitations, the majority of these electrolyte systems, however, cannot take place of the cyanide baths totally.

Our research group has developed cyanide-free baths for gold and silver electroplating by using 5, 5' – dimethylhydantoin (DMH) as one of the complex agents [7, 8]. From previous studies, we find that the features of complexation and adsorption of DMH are two key factors that influence the cathodic deposition processes of gold and silver. In addition, the nature of gold, silver, and copper is similar to some degree. To our knowledge, two patents [9, 10], whose statements are very vague, have claimed to use DMH as one optional agent for copper electroplating, but no related literatures or detailed studies has been found. Therefore, we are interested to investigate solutions containing DMH from the electrochemical point of view and develop a potentially robust bath.

In order to obtain copper layers with good adhesion on carbon steel substrate, one key point is to prevent the formation of a copper immersion coating on the steel substrate. However, that is not the only factor decreasing the adhesion except for poor cleaning and pretreatment [11]. As steel substrate is very easy to be oxidized in air and water, the thin passive film that forms before the electrolytic cell is powered on also plays a significant role in decreasing the adhesion between copper electrodeposits and steel substrate [11-13]. Hydantoin and its derivatives that are, as a rule,

used as drugs can coordinate with many metal ions, including Au, Ag, Co, Ni, Cu, and Zn ions [14, 15]. The formation of copper-DMH complex may prevent the immersion coating. By forming an adsorbed layer on metal surface, some organic molecules containing polar groups such as organic N, amine, S, and OH groups can inhibit corrosion of iron in acid [16]. Hydantoin also has a polar group (N-heterocyclic) and some hydantoin derivatives have been confirmed to be able to inhibit corrosion of iron in acid solution [17, 18]. So we suppose that DMH may also be adsorbed on the carbon steel surface, which can influence the electrodeposition process so that the adhesion between electrodeposits and the steel substrate will be enhanced. Molecular dynamic simulation is able to predict and investigate the adsorption behavior and the interaction energy of organic molecules on metal surfaces [19, 20]. Although with DMH as the only complex agent the immersion coating could be prevented efficiently at high concentration ratio of DMH to copper ions, the current efficiency (CE) in our experiments was too low to be acceptable. For this reason we chose citrate as the second complex, which can coordinate stably with cupric ions and has be studied widely [21-24].

In the present work we investigated the cathodic discharge processes and kinetic features of solutions in the presence of only DMH, only citrate, and both as complex agents with cyclic voltammetry and sample current voltammetry. Chronopotentiometry and chronoamperometry were employed to explore the initial process of the electrodeposition, including the nucleation growth and desorption of DMH molecular, whose adsorption behavior on steel substrate was revealed by using molecular dynamic simulation. Cathodic polarization was demonstrated by potentiodynamic cathodic polarization curves on the platinum rotating disk electrode. The CE of

the baths and the surface morphology, crystal structure, and the adhesion of copper layers electrodeposited on carbon steel substrate were also discussed.

2 Experimental

2.1 Preparing baths and electrochemical measurements

All reagents were of analytical grade. Distilled water was used throughout. The baths were composed of $CuSO_4 \cdot 5H_2O$ as the main salt, DMH and citrate (potassium citrate) as complex agents, and K_2CO_3 as the buffer. Sulphuric acid and sodium hydroxide solutions were used to adjust the pH of the baths. The composition of the main solutions in the experiments is presented in Table 1. The pH was 9 and the temperature 50℃ if not mentioned specifically.

Table 1 the Composition of main solutions used in this work

Solution NO.	Concentration (M)			
	$CuSO_4 \cdot 5H_2O$	DMH	citrate	K_2CO_3
Sp1	0.1	0.0	0.6	0.3
Sp2	0.1	0.2	0.6	0.3
Sp3	0.1	0.5	0.6	0.3
Sp4	0.1	0.5	0.0	0.3
Sp5	0.1	0.5	0.3	0.3
S1	0.1	0.0	0.3	0.3
S2	0.1	0.2	0.3	0.3
S3	0.1	0.4	0.3	0.3
S4	0.1	0.2	0.1	0.3
S5	0.1	0.2	0.5	0.3
S6	0.1	0.2	0.3	0.0
S7	0.1	0.2	0.3	0.5

All electrochemical measurements were conducted in a typical three-electrode cell connected to a potentiostat/galvanostat. A glass carbon (GC) and platinum (Pt) electrode (φ= 3 mm) and a carbon steel disk (φ= 5 mm) embedded in Teflon was used as the work electrode for cyclic voltammetry, chronoamperometry, and chronopotentiometry measurements. A glass carbon and a platinum rotating disk electrode (RDE, φ = 5 mm) as the work electrodes for polarization curves

and CE measurements. The carbon steel electrode was polished to mirror finish immediately prior to the measurements. A platinum plate was employed as the counter electrode and a saturated calomel electrode (SCE) as the reference electrode for all electrochemical experiments.

The deposition/stripping method based on constant-current chronopotentiometry [25-27] was employed to estimate the current efficiency. Firstly, copper electrodeposition was performed at constant cathodic current density for 10 minutes. Then stripping was carried out at constant anodic current density to oxidize the electrodeposits in the electrolyte containing 300 g/L NH_4NO_3. The potential was monitored as a function of time when stripping (One example of the potential *vs*. time curves obtained by oxidizing the copper deposits is shown in Figure S1 of the Supplementary Materials). The time at which the potential rose to 1.0 V *vs*. SCE was chosen as the end point of the oxidization process for all experiments. The CE was calculated by using equation(1).

$$\mathrm{CE} = \frac{i_a \times t_a}{i_c \times t_c} \tag{1}$$

Where i_a and i_c are anodic oxidation and cathodic reduction current, respectively. t_a and t_c are the time used for oxidation and reduction, respectively. Here the CE of the oxidation process was assumed to be 100%.

A cell consisting of a copper sheet (5×5 cm) as the anode and a carbon steel sheet (3×3 cm) as the cathode was employed for electroplating experiments. All electroplating experiments were performed at galvanostatic conditions with relative strong mechanical agitation (around 200 rpm with an agitator blade).

2.2 Molecular dynamic simulation

Molecular dynamic simulations were realized in simulation boxes with periodic boundary conditions using Materials Studio (from Accelrys Inc). The boxes consisted of a surface (cleaved

along the (111) plane for ferrum and along the (111) plane for copper) and a liquid phase. The liquid phase contained water molecules with density of 1 g/cm^3 and several organic molecules in every box. All molecular dynamic simulations were carried out at 323 K, NVT ensemble, and COPMASS force field with a time step of 1 fs and simulation time of 500 ps. The interaction energy $E_{\text{interaction}}$ between the metal surface and one organic molecule was calculated by the equation(2):

$$E_{\text{interaction}} = \frac{1}{n}(E_{total} - E_{polymer} - E_{surface}) \quad (2)$$

Where E_{total} is the total energy of the metal crystal together with the adsorbed organic molecules, E_{surface} and E_{polymer} the total energy of the metal surface and free organic ions, respectively, and n is the number of the organic molecules simulated in the box. The binding energy is the negative value of the interaction energy.

2.3 Characterizing copper layers

Environmental scanning electron microscope (SEM, Quanta 200F) was employed to observe the surface morphology and cross-sections of copper layers. Crystal structure was revealed by X-ray diffraction (XRD, PANalytical X'Pert PRO).

It is very difficult to measure adhesion quantitatively and "yes or no" test procedure is used in many cases even today [12]. Bend test, cross-hatch test, and thermal shock test can be utilized to evaluate the adhesion of electroplated copper layers on carbon steel substrate [12]. In this work, the sample sheet was bent to and fro through an angle of ±90° until it was broken into two parts for bend test. A harden steel engraver with angel of 30 degree was used to cross-hatch a mesh pattern of 1 to 3 mm in length for cross-hatch test. For thermal shock test samples were heated in an oven to 250℃ and then immersed into cool water (25℃) suddenly. The carbon steel substrate was

polished to a mirror finish, then degreased, and activated in weak acid solution before electrodeposition. After electroplating copper in the investigated baths for 30 minutes, electrodeposition of another 30 minutes was performed in a typical sulfate baths to make the copper layers thick enough. Then the adhesion was evaluated with the three methods mentioned above.

3 Results and discussion

Three types of electrochemical measurements including cyclic voltammetry, chronoamperometry, and chronopotentiometry were employed to analyse the cathodic discharge process of copper in three solutions, Sp4 with only DMH, Sp3 with only citrate, and Sp1 with both DMH and citrate as the complex agents. Cyclic voltammetry with various switch potentials and various scan rates were realized to investigate the reactions and their kinetic features. The sample current voltammetry with the simple analysis method, proposed by Michael V. Mirkin and Allen J. Bard [28], were used to obtain the kinetic parameters of the Pt or GC electrode in the solution with only DMH or only citrate as the complex agent. Diffusion coefficient was calculated by fitting the current *vs*. time curves according to Contrell equation. Nucleation was compared with the nucleation models proposed by Scharifker and Hills, which is relatively simple and used most frequently [29, 30].

3.1 **Cyclic voltammetry for the discharge processes**

3.1.1 Various switch potentials

Cyclic voltammograms of the Pt electrode from 1.0 V to various switch potentials (− 0.40, − 0.60, − 0.80, − 1.00, − 1.10, − 1.15, − 1.30, and − 1.50 V) *vs*. SCE in solution Sp4 with only DMH as the complex agent is shown in Figure 1. All the potential scan was initially swept toward the

negative direction from the rest potential at the scan rate of 50 mV/s. In the range from 1.0 V to − 1.5 V in Figure 1 (a), three cathodic peaks (C1 (− 0.20 V), C2 (−0 .85 V), C3 (− 1.24 V)), and five anodic peaks (A1 (− 0.27 V), A2 (− 0.17 V), A3 (− 0.04 V), A4 (0.23 V), A5 (0.70 V)) can be observed. The peak C1 shifts negatively in the 2nd cycle comparing with the 1st cycle, which is attributed to the copper deposited on the Pt electrode but not stripped totally in the 1st cycle, as copper covering the Pt electrode was observed macroscopically after five cycles. When the switch potential is − 0.40 V, − 0.60 V, and − 0.80 V, the curves have only one cathodic peak C1 and one anodic peak A4 in Figure 1 (b). The anodic A1 appears when the scan switches at − 1.00 V, and the anodic A2 appears when the scan switches at − 1.10. A3 appears in the curves with the switch potential of − 1.15 V. The curves with the switch potential of − 1.30 has all the five anodic peaks.

We assume that the main copper-DMH species is $[Cu(DMH^{-})_3]^{-}$ in the solution Sp4, as the three copper-DMH complexes are $[Cu(DMH^{-})]^{+}$, $[Cu(DMH^{-})_2]$, and $[Cu(DMH^{-})_3]^{-}$, of which the formation constants ($\log_{10}(\beta)$) are 4.3, 8.2, 12.1, respectively [14] and the pH of the solution Sp4 was 9. Although no report about complexation between Cu^{+} and DMH except one patent [10], which gives no definite data, has been found, here we assume that the coordination of Cu^{+} and DMH forms $[Cu(DMH^{-})]$. According to all the results above, we can conclude that the main copper-DMH species is discharged by two steps, although the voltammograms have three cathodic peaks. The first cathodic peak C1 is referred to the first discharge step from Cu^{2+} to Cu^{+} as equation(3). Corresponding to the C1, the anodic peak A4 is attributed to the oxidation of Cu^{+}. The second cathodic peak C2 is related to the second discharge step from Cu^{+} to Cu^{0} as equation(4), and the anodic peak A1 is attributed to the oxidation of Cu^{0}. Different to the related report of literatures [31], a sharp cathodic peak, C3, appears after the second one. This behaviour

may be related to a catalytic reaction. The small amount of copper electrodeposited at C2 accelerates the discharge of Cu^+. Because the second cathodic peak C2 is more like a platform, indicating the diffusion of Cu^+ did not reach limitation after peak C2. Moreover, the much larger area at the anodic peaks of the curves with peak C3 means that much more copper is deposited at peak C3. The anodic peaks A2, A3, and A5, which are not easy to define, may be attributed to the production of hydroxides or oxides that may be adsorbed or forming soluble species [32].

$$\left[\mathrm{Cu}\left(\mathrm{DMH}^-\right)_3\right]^- + e^- \rightarrow \left[\mathrm{Cu}\left(\mathrm{DMH}^-\right)\right] + 2\mathrm{DMH}^- \quad (3)$$

$$\left[\mathrm{Cu}\left(\mathrm{DMH}^-\right)\right] + e^- \rightarrow \mathrm{Cu}^0 + \mathrm{DMH}^- \quad (4)$$

Cyclic voltammograms of the GC electrode from 1.0 V to various switch potentials (− 1.00, − 1.30, − 1.35, − 1.40, and − 1.5 V) *vs*. SCE in solution Sp4 with only DMH as the complex agent is shown in Figure 2. All the potential scan started in the negative direction from the rest potential at the scan rate of 50 mV/s. The voltammogram with the potential range from 1.0 V to − 1.5 V *vs*. SCE in Figure 2 (a) has two cathodic peaks (C1 (− 0.30 V), C2 (− 1.45 V)), and four anodic peaks (A1 (− 0.30 V), A2 (− 0.20 V), A3 (− 0.02 V), A4 (0.15 V)). Not like that on the Pt electrode, the peak C1 does not shift in the 2nd cycle comparing with the 1st cycle. But the initial point of the second peak C2 shifts positively, which also is attributed to the copper deposited but not stripped totally in the 1st cycle. The voltammogram has a large peak separation and crossover on the cathodic branches, indicating the presence of nucleation and growth processes [29], whereas the voltammogram on the Pt in Figure 1 does not have this feature. When the switch potential is − 1.00 V and − 1.30 V, the curves have only one cathodic peak C1 and one anodic peak A4 in Figure 2 (b). The anodic A1 and A2 appear when the scan switches at −1.35 V, and the anodic A3 appears when the scan switches at − 1.40, at the same time the crossover related to the nucleation also appears.

From these results, the discharge process of the main copper-DMH species on the GC electrode also has two steps but is different to that on the Pt electrode. The cathodic peak C1 and the anodic peak A4 are referred to the first step, Cu^{2+} to Cu^{+} as equation(3), The cathodic peak C2 and the anodic peaks A1 and A2 are attributed to the second step, Cu^{+} to Cu^{0} as equation(4). Similar to the condition on the Pt electrode the anodic peak A3 may be attributed to the production of hydroxides or oxides.

Cyclic voltammograms of the GC electrode from 1.0 V to various switch potentials (− 0.60, − 0.93, − 1.35, and − 1.5 V) *vs*. SCE in solution Sp1 with only citrate as the complex agent is shown in Figure 3. All the potential scan started in the negative direction from the rest potential at the scan rate of 50 mV/s. The voltammogram with the potential range from 1.0 V to −1.5 V *vs*. SCE in Figure 3 (a) has one big cathodic peaks (C3 (− 1.20 V)) and four small cathodic peaks (C1 (− 0.925 V), C2 (− 0.99 V), C4 (− 1.33 V), C5 (− 1.60 V)) and four anodic peaks (A1 (− 0.285 V), A2 (− 0.09 V), A3 (− 0.00 V)). No peak shift can be observed in the 2nd cycle comparing with the 1st cycle. The peak A2 can be observed in all the three curves with the switch potentials of − 0.60, − 0.93, − 1.35 V in the zoom view of Figure 3 (b). The peak of A1 and A3 cannot be observed clearly in the curves with the switch potentials of − 0.60, − 0.93, thus it is not easy to determine whether the two curves has the two peaks. The curves with the switch potential of − 1.35 V have all the three anodic peaks, which can be observed clearly in Figure 3 (b).

The cathodic peak C1, C3, C4, and C5 is very small and difficult to define, here we only discuss the predominant cathodic peak C2. According to the reports of Rode, S., et al [22], the predominant copper-citrate species is the $[Cu_2(Cit_2H_{-2})]^{4-}$ dimer with the formation constant (log10(β)) of 5.1, and the discharge process of the $[Cu_2(Cit_2H_{-2})]^{4-}$ has two steps with an adsorbed blocking

intermediate, $[Cu_2(Cit_2H_{-2})]_{ads}^{6-}$. Considering the discussion of the results in Figure 1 and 2, it can be inferred that the anodic peaks A2 and A3 in Figure 3 (b) are referred to the oxidation of Cu^+ and the peak A1 to the oxidation of Cu^0. In the voltammogram with the switch potential of − 0.60 V, although no obvious cathodic peak can be observed, but the anodic peak proves that the first discharge step exists as equation(5). Therefore, the discharge of $[Cu_2(Cit_2H_{-2})]^{4-}$ in our experiments also has the two steps. The cathodic peak C2 and the anodic peak A1 are attributed to the reaction demonstrated by equation(6). In addition, the cyclic voltammetry at various scan rates combining with the sample current voltammetry confirms that the discharge in this work accords with the mechanism proposed by Rode, S., et al.

$$[Cu_2(Cit_2H_{-2})]^{4-} + 2e^- \rightarrow [Cu_2(Cit_2H_{-2})]_{ads}^{6-} \quad (5)$$

$$[Cu_2(Cit_2H_{-2})]_{ads}^{6-} + 2e^- + 2H_2O \rightarrow 2Cu + 2Cit^{3-} + 2OH^- \quad (6)$$

Cyclic voltammograms of the GC electrode from 1.0 V to − 1.25 and − 1.5 V *vs*. SCE in solution Sp3 with both DMH and citrate as the complex agents is shown in Figure 4. All the potential scan started in the negative direction from the rest potential at the scan rate of 50 mV/s. Two cathodic peaks (C1 (− 0.90 V) and C2 (− 1.40 V), four anodic peaks (A1 (− 0.26 V), A2 (− 0.15 V), A3 (− 0.05), and A4 (− 0.17)), and a nucleation crossover are observed in the voltammogram with the range from 1.0 V to − 1.5 V. Whereas only one cathodic peak C1 and two anodic peak exist in the voltammogram with the range from 1.0 V to − 1.25 V. These results indicate that the predominant cupric complexes also discharge by two steps with C1 and A3, A4 referred to Cu^{2+} to Cu^+ and C2 and A1, A2 referred to Cu^+ to Cu^0. This agrees with the discharge processes of cupric complexes in solution with only DMH or citrate as the complex, as the feature of the voltammogram in Figure 3 is very close to the synthesis of the ones in Figure 1(a) and Figure

2 (a). In addition, Peak C1 shifts negatively and peak C2 is smoother in the 2nd cycle comparing with that in the 1st cycle in Figure 3, which is also observed in the curves obtained from the former two solutions. This results from that the surface of the electrode is changed by the potential scan in the 1st cycle.

3.1.2 Various scan rates

Voltammetry measurements at various scan rates were conducted in the three solutions, Sp4, Sp1, and Sp3. The results are presented in Figure 5. To keep consistency of the electrode surface in the experiments of this part, the electrode were pretreated by voltammetry until no peak shift occurs in the last two cycles before every voltammetry measurement was performed. Figure 5 (a) and (b) show the voltammograms at various scan rates of the Pt and GC electrode, respectively, in solution Sp4 with only DMH as the complex agent. Figure 5 (c) and (d) show the voltammograms of the GC electrode in solution Sp1 and Sp3, respectively. The potential scan in Figure 5 (a) and (b) falls in the range in which only the first step discharge can happens, and the potential scan in Figure 5 (c) and (d) falls in the range of the two step discharge. All the voltammograms in the four figures have the features of the irreversibility reaction: the relationship of the peak current density (i_p) and the square root of the scan rate ($v^{1/2}$) is linear, and the peak potential E_p shifts negatively with the increase of the scan rate. But of the four plots of i_p *vs*. $v^{1/2}$ only the one in Figure 5 (c) has the intercept of zero, and the diffusion coefficient calculated from the voltammetry according to equation(7) is not in accord with the results from chronoamperometry (see Figure 3). The transfer coefficients (α) listed in Figure 3 was also calculated from the cyclic voltammetry according to equation(8) (detail data is listed in table S1 of the supplementary materials). The α calculated from the cyclic voltammetry of the Pt electrode in solution Sp4 with only DMH as the complex agent is

in accord with the value from the sample current voltammetry. The α calculated from the cyclic voltammetry of the GC electrode in solution Sp1 with only citrate as the complex agent is also very close to the one from sample current voltammetry, when the number of transfer electron n is 2, which confirms the validity of equation(5). These results allow us to speculate that the reaction of copper-DMH complex on the GC electrode is much more complex than that in equation(3), considering that the α calculated from the cyclic voltammetry of the GC electrode in solution Sp4 is a half of the one from sample current voltammetry when n = 1. By the way, no significant data was obtained from the polarization curves on a GC rotating disk electrode with the slow san rate of 1 mV/s. The electrodeposition process on the GC electrode seems controlled by the charge transfer process in solution Sp4 and Sp3 while exhibits features of the diffusion control in solution Sp1 (see Figure S2 to S5 of the supplementary materials). The data from solution Sp1 was used to calculate the diffusion coefficient based on the kinematic viscosity of 0.01 cm^2/s according to the Koutecký –Levich equation, which, however, departures largely to the one from the cyclic voltammetry. The value, 61.12×10^{-7} $cm^2 \cdot s^{-1}$, obtained from the rotating disk electrode is more than that reported, 21.30×10^{-7} $cm^2 \cdot s^{-1}$ [33].

$$j = 0.04858FC_O^* D_O^{1/2} v^{1/2} (\frac{\alpha F}{RT})^{1/2} \tag{7}$$

$$| E_p - E_{p/2} | = \frac{1.857RT}{\alpha nF} \tag{8}$$

Where j is the current density, F the Faraday Constant, C_O^* the mole concentration of the electroactive species, assumed to be 0.1 M in this work, D_O the diffusion coefficient of the electroactive species, v the scan rate, R the gas constant, T the thermodynamic temperature, E_p the peak potential, and $E_{p/2}$ is the potential where the current is at half the peak value.

3.2 Chronoamperometry

3.2.1 Sample current voltammetry for kinetic parameters

Chronoamperometry was used to get the sample current voltammograms (The original current density *vs*. time curves are presented in figure S6, to S8 of the supplementary materials). The sample current voltammogram of the Pt electrode in solution Sp4 is shown in Figure 6 (a) (and the ones of the GC electrode in solution Sp4 and Sp2 is presented in Figure S9 and S10 of the supplementary materials). The kinetic parameters based on the database proposed by Mirkin, M. V. and A. J. Bard [28] are presented in Table 2. Simple linear interpolation and the temperature coefficient, 298/T, for $E_{1/4}-E_{1/2}$ and $E_{1/2}-E_{3/4}$ have been employed in the analysis. Figure 6 (b) is the Tafel curve based on the data of the sample current voltammogram in Figure 6 (a). The α calculated from the Tafel curve is very close to the ones from the database, which confirms the validity of the analysis proposed by Mirkin, M. V. and A. J. Bard. However, the conditional (formal) potential $E°'$ calculated may be invalid, as they are smaller than the rest potentials of the systems. The standard rate constant $k°$ was calculated by using equation(9) [28].

$$k^0 = \lambda\sqrt{D_0 / (\pi t)} \tag{9}$$

Where λ is the dimensionless rate constant, $\lambda = k°/D_O$ and t is the time at which the current density is used for the sample current voltammogram.

Table 2 Kinetic parameters calculated from the sample current voltammetry based on the database proposed by Mirkin, M. V. and A. J. Bard

	$E_{1/4}-E_{1/2}$ (mV)	$E_{1/2}-E_{3/4}$ (mV)	λ	$k°$ cm/s	nΔE°' (mV)	E°' (mV)	α	α_{Tafel}	α_{CV}
Pt in Sp4	42	43	0.17	1.04×10^{-5}	72	−0.02	0.65	0.61	0.64
GC in Sp4	67	66	0.20	1.23×10^{-5}	106	0.01	0.41	0.41	0.20
GC in Sp1	84	81	0.20	5.10×10^{-5}	128	−0.48	0.34	0.30	0.34

* $D_{Cu^{2+}}$ *(10^{-7} $cm^2 \cdot s^{-1}$): 3.54 for Pt electrode in Sp4, 3.61 for GC electrode in Sp4, and 61.12 for GC electrode in Sp1.* α_{Tafel} *was obtained from the data of sample current voltammetry according to Tafel equation.* α_{CV} *was calculated from the voltammetry in Figure 5 according to equation(1.8), of which the number of transfer electron n = 1 for Pt electrode in Sp4, n = 1 for Pt electrode in Sp4, n = 2 for GC electrode in Sp1.*

Obviously, the Pt and GC electrode in solution Sp4 with only DMH as the complex agent have different α value, indicating different discharge mechanisms on the two electrodes. This is in accord with the results of the cyclic voltammetry, as the cyclic voltammograms on the two electrodes have different shapes.

3.2.2 Contrell equation fitting for diffusion coefficient

The plots of j *vs*. $t^{-1/2}$ of the Pt and GC electrodes in solution Sp4 with only DMH as the complex agent is shown in Figure 7. The current *vs*. time curves with the potential stepping from 0.2 V to −0.16 V *vs*. SCE was used to fitting the plots of j *vs*. $t^{-1/2}$, and equation(10) and (11) are the two equations derived from the intercepts and slopes of the two plots. Theoretic curves based on equation(10) and (11) match very well with the curves measured as shown in the zoom view of Figure 7. The diffusion coefficients, calculated from the two plots according to Contrell equation [34, 35], is very close and listed in Table 3. No significant data was obtained from the current *vs*. time curves of the GC electrode in solution Sp1 because the nucleation feature appears early at the relative small step potential (see Figure S8 of the supplementary materials).

$$j = 19.063 + 32.417t^{1/2} \tag{10}$$

$$j = 20.839 + 32.727t^{1/2} \tag{11}$$

Table 3 Diffusion coefficients calculated from cyclic voltammetry and chronoamperometry

$D_{Cu^{2+}}$ (10^{-7} cm$^2 \cdot$ s^{-1})	Pt in Sp4	GC in Sp4	GC in Sp1
Cyclic voltammetry	1.59	7.06	181.60
Chronoamperometry	3.54	3.61	–
RDE	–	–	61.12

3.2.3 Nucleation modelling

Potentiostatic current transients presented in Figure 8 were recorded in the potential ranges of the electrochemical deposition of copper on the GC electrode from solutions Sp4 (Figure 8 (a)), Sp1 (Figure 8 (b)), and Sp3 (Figure 8 (c)). The potential range used agrees with the results of the

previous cyclic voltammetry. All the current transients have the following characteristic features: an abrupt drop followed by an increase in the cathodic current density up to a maximum j_{max} at t_{max}, which is related with the crystal nucleation and growth processes, then a decaying in the current density after t_{max}, converging to the limiting current density corresponding to linear diffusion of the electroactive species to a planar electrode, and a bigger j_{max} and a shorter t_{max} with a more negative step potential.

The SH nucleation models classify the nucleation and crystal growth in three dimensions (3D-dc) controlled by diffusion into two types: the instantaneous process (equation(12)) with simultaneously activated active sites followed by a slow growth of nuclei, and the progressive process (equation(13)) with continually formed active sites followed by a fast growth of nuclei [36, 37]. The comparisons of the experimental curves to the dimensionless theoretical curves of the three solutions are presented in Figure 8 (A), (B), and (C). At all step potentials in this work, the curves (− 1.300 to − 1.388 V) in Figure 8 (A) from solution Sp4 with only DMH as the complex agent and the curves (− 1.25 to − 1.35 V) in Figure 8 (B) from solution Sp3 with both DMH and citrate as the complex agents show a great agreement with the progressive nucleation process before t_{max}, while departure downward after t_{max}, which becomes stronger with a more negative step potential. According to Floate, S., et al [37], the concomitant hydrogen evolution or the rapid replenishment of electroactive species through hemi-spherical diffusion to growth centres may contribute to the departure. The former exerts a greater effect with more negative step potential while the latter influences more with less negative step potential. No departure is observed in the curves (− 1.300 to − 1.388 V) in Figure 8 (C) from solution Sp4 with only citrate as the complex agent, which also exhibits an agreement with the progressive nucleation process. It can be concluded that DMH

have a stronger influence on the nucleation and crystal growth process of copper on the GC electrode in solution Sp3 with both DMH and citrate as the complex agents in the experimental composition.

$$(\frac{j}{j_m}) = 1.9542(\frac{t}{t_m})^{-1}\{1 - \exp[-1.2564(\frac{t}{t_m})]\}^2 \quad (12)$$

$$(\frac{j}{j_m}) = 1.2254(\frac{t}{t_m})^{-1}\{1 - \exp[-2.3367(\frac{t}{t_m})]\}^2 \quad (13)$$

3.3 The adsorption of DMH molecules on steel substrate

3.3.1 Molecular dynamic simulation

Molecular dynamic simulations were conducted to reveal the adsorption behaviours of DMH and citrate acid molecules on the Fe (111) and Cu (111) surface. All the simulations had run for 500 ps in which the computed systems had reached a steady state (as shown by the energy and potential *vs*. time curves in supplementary materials). The results are shown in Figure 9 and the interaction energy $E_{\text{interaction}}$ between the organics and the metal surface are listed in Table 4. All DMH molecules simulated, which are placed randomly in the boxes before computing, get close to the surface of Cu (111) and Fe (111) at the end of the simulation. Two of the four DMH molecules simulated have the planes of their heterocycle parallel to the Cu (111) surface, and the other two make the planes of their heterocycle perpendicular to the Cu (111) surface. While the planes of the heterocycle of all the four molecules simulated are parallel to the Fe (111) surface. The adsorption behaviours simulated of DMH^- (DMH molecule lacking one proton), citrate acid molecule (Cit), Cit^- (citrate acid molecule lacking three protons), and hydrogen cyanide molecule on Fe (111) and Cu (111) surface are not presented in the paper (See Figure S14 to S23 of supplementary materials). According to Table 4, both DMH and DMH^- have a stronger adsorption on Fe (111) surface than that on Cu (111), surface and both Cit and Cit^- also have a stronger

adsorption on Fe (111) surface than that on Cu (111) surface. In fact, Cit and Cit^- did not get close to the surface of Cu (111) at the end of the simulation and the $E_{binding}$ between Cit^- and Cu (111) surface is negative. In addition, neutral molecules, no matter DMH or Cit, have a larger $E_{binding}$ than molecules with negative charge on both the Fe (111) and Cu (111) surface.

Table 4 Interaction energy between the organic molecules and metal surfaces involved in Molecular dynamic simulation

	E_{total} (kJ/mol)	$E_{surface}$ (kJ/mol)	$E_{polymer}$ (kJ/mol)	$E_{binding}$ (kJ/mol)
DMH on Fe (111)	259862399.10	259865287.90	−1554.32	333.64
DMH^- on Fe (111)	255802131.80	255802937.10	231.43	259.16
Cit on Fe (111)	259863609.30	259865356.90	−1013.50	183.53
Cit^- on Fe (111)	259867179.60	259865287.90	1744.84	−36.70
HCN on Fe (111)	259865055.30	259865356.90	42.18	42.97
DMH on Cu (111)	2078040.71	2080417.59	−1554.00	205.72
DMH^- on Cu (111)	2080252.76	2080417.59	266.67	107.88
Cit on Cu (111)	2079465.50	2080417.59	−923.67	7.10
Cit^- on Cu (111)	2083831.67	2080417.59	3294.77	−29.83
HCN on Cu (111)	2080139.38	2080417.59	43.83	40.25

3.3.2 Chronopotentiometry

Chronopotentiometry was used to investigate the initial stage of copper electrodeposition process on the carbon steel substrate in S2. The potential *vs*. time curves obtained from S2 at various current densities and from background solutions with and without DMH are shown in Figure 10. The background solution is composed of 0.0 or 0.2 M DMH, 0.3 M citrate, and 0.3 M K_2CO_3. These curves (10, 15, 20, 25 mA/cm^2) are generally characterized by five stages: (1) an abrupt potential drop which can be ascribed to the ohmic potential drop, (2) a slow decrease of the potential which can be attributed to the charging of the double-layer capacitance, (3) a negative potential peak, (4) another slow decrease of the potential which can be ascribed to the decrease of the concentration of the reactant at the interface caused by the decay of the diffusion process, and lastly (5) a potential platform at which copper electrodeposition and hydrogen evolution occur simultaneously. But the curves obtained at 5 mA/cm^2 does not have the fifth stage and ends at a

potential platform at which only the discharge of copper complexes occurs. The results indicate that there is a strong hydrogen evolution when copper is electrodeposited galvanostatically at above 10 mA/cm^2.

The negative potential peak, as observed clearly from the inset in Figure 10, at the third stage may be ascribed to the reduction of the passive film on the surface of the steel electrode [13, 38, 39] or the desorption of DMH molecules adsorbed on the steel electrode. The latter assumption is confirmed by the potential curves from the background solutions without and with DMH (curve (a) and (b) figure 5), as the potential *vs*. time curve (b) from the background solution with DMH also has a negative potential peak initially although the peak value is lower than that of the curves from the solution containing cupric ions. However, no negative potential peak can be observed in the curve (a) from the background solution without DMH.

3.4 Cathodic polarization curves

The cathodic polarization curves with the Pt RDE as the work electrode at 300 rpm were obtained from alkaline DMH/citrate baths with various compositions and conditions. The scan rate for all curves was 1 mV/s. Cathodic polarization curves for copper electrodeposition with the effect of adding increasing amounts of DMH and citrate are shown in Figure 11 (a) and (b), respectively. Two reduction waves and a peak around − 0.65 V can be observed in curves from solutions in the presence of DMH. The peak current density of the first wave, associating with the discharge of copper-DMH complex according to the cyclic voltammograms, rises with the increment of the DMH concentration, while that descends with increasing the citrate concentration.

Figure 11 (a) shows how the polarization is influenced by increasing the amount of DMH in solutions (Sp2, Sp3). In the solution (Sp1) in the absence of DMH there is no significant current before about − 0.95 V, indicating a big overpotential. The current density rises linearly between − 0.95 to − 1.35V with increasing cathodic potential and then reaches the limiting current plateau. However, the extent of the cathodic polarization falls with increasing the DMH concentration. According to literature reports [14, 22], the stability constants (log10 (β)) of copper-DMH and copper-citrate complexes in our experimental conditions were very close. Therefore, with adding DMH into solutions, there was a competition between DMH and citrate to coordinate with cupric ions, as the stability constants of the two complexes were so similar. These results demonstrate that it is easier to discharge the copper-DMH complex than the copper-citrate complex. It can also be observed that increasing DMH concentration decreases the limiting current density, indicating that copper-DMH complex diffused slower than copper-citrate complex, in agreement with the previous results.

The effect of the citrate concentration (Sp3, Sp4, Sp5) on cathodic polarization is given in Figure 11 (b). Both the cathodic polarization and the limiting current density are decreased significantly with addition of citrate. This results from a more difficult discharge as more copper-citrate complexes formed. Figure 11 (c), with data from solution S2 at 50℃, shows that the overpotential decreases a little when pH is raised from 8.5 to 9, but no significant difference is observed in the limiting current density at various pH (8.5, 9, 10.5). The influence of temperature on cathodic polarization measured in solution S2 at pH 9 is shown in Figure 11 (d). The polarization falls and the limiting current density rises with the increment of temperature from 25

to 60 ℃. This trend can be ascribed to the effect of temperature on the diffusion coefficient, which goes up with increasing temperature.

3.5 **Current efficiency**

The CE as a function of current density at 40 and 50 ℃ is presented in Figure 12. The investigated bath has a CE above 70% at 50 ℃, which is similar to the CE of classical cyanide baths [1]. The CE of the solution S2 in Figure 12 (a) falls with increasing the current density from 5 to 15 mA/cm^2, then keeps stable from 15 to 25 mA/cm^2, and lastly tends to fall again after 25 mA/cm^2. This trend is expected due to simultaneous hydrogen evolution reaction which is enhanced by increasing current density and confirmed by the set of potential *vs*. time curves in Figure 10. Comparing curve (a) at 50℃ with (b) at 40℃ in Figure 12 shows that the CE increases with evaluating temperature because of the influence of temperature on the diffusion coefficient. This result is in correspondence to the data in Figure 11.

3.6 **Characteristics of copper electrodeposits**

3.6.1 Morphology

The surface morphology of copper layers electrodeposited for 30 min at 15 mA/cm^2 from solutions with various concentrations of DMH, citrate, and K_2CO_3 and at various pH was observed by using SEM and the images are given in Figure 13 (More images are presented in Figure S11 and S12, and the thickness of the layers calculated from the cross-sectional SEM images like Figure 15 are listed in table S2 of supplementary materials). The surface of the copper layer obtained from S1 that did not contain DMH is dark and rough in Figure 13 (1), and clusters with cracks in between can be observed. That is because the citrate concentration is too low to reduce free cupric ions to an adequately low level by coordinating. With addition of DMH into the bath

(S2), the cracks between the clusters disappear and the layer becomes finer with small islands dispersing on the surface in Figure 13 (2). The small islands, which can also be observed on the other layers, may be ascribed to the discharge of one species which are easily reduced. The layer is denser and smoother but too thin (2.50 um) when the DMH concentration is 0.4 M.

From the images of Figure 13 (3) and (4), with increasing the citrate concentration the copper layer is first compact with tremendous amounts of small islands on the surface, and then has some dents that may be attributed to hydrogen evolution, and lastly become very smooth. And the thickness of the layer increases at first and then decreases on further addition of citrate, which is related to the coordinating environment in the solution. The K_2CO_3 concentration also has a significant effect on the surface morphology in Figure 13 (5) and (6). The layer become smoother with addition of K_2CO_3, compared with that obtained from S6 without K_2CO_3. When the K_2CO_3 concentration is at 0.5 M, the dents become holes and the islands are more disperse, which is attributed to strong hydrogen evolution. And the thickness decreases with the increase of the K_2CO_3 concentration. These results indicate that K_2CO_3 also influences the coordination environment and the electrodeposition process. On the other hand, the layer becomes smoother and the thickness increases with increasing pH. The amount of islands is small but some dents can be observed at pH 9. In addition, the image of the copper layer electroplated from the bath with only DMH as complex agent is not presented, because to prevent the immersing coating of copper, adequate amount of DMH has to been used, but no copper layer can be obtained in a large current density range (5~ 40 mA/cm^2) even at the DMH concentration of 0.4 M.

3.6.2 Crystal strucutre

XRD was used to reveal the structure and calculate the average crystal sizes of the copper layers electroplated from different baths and at different pH. The main peaks in the spectra match very well with the pattern of a standard powder copper sample (PDF#4-0836) (see the Figure S14 of supplementary materials), indicating that the copper layer has a crystalline cubic structure. The average crystal size calculated from the intensity of peak (a) and (b) by using Scherrer equation is about 30 nm (see table S5 of supplementary materials) [40], which is nearly 70% smaller compared to those (91 nm) reported for copper electrodeposits obtained from an additive-free acid copper sulfate bath [41]. The copper layer deposited from solution with only citrate as the complex agent prefers orientation (111) in the crystals in Figure 14 (a). With addition of DMH into the solution, orientation (111) of the crystals becomes preferable in orientation (200). This result agrees with Figure 14 (b), in which the peak of orientation (111) becomes reversely stronger than that of orientation (200) with the increase of the citrate concentration from 0.1 M to 0.5 M. The behaviors of the crystal orientation with changing solution compositions confirm the competitive relationship between DMH and citrate in coordination with cupric ions, as more citrates can form more copper-citrate complex, which predominate the discharge and produce more crystals with orientation (111). Although not changed, the preferable crystal orientation (200) becomes stronger with the increase of the concentration K_2CO_3 while weaker with the increase of pH. This indicates that more K_2CO_3 and lower pH enhance the discharge of copper-DMH.

3.6.3 Adhesion on steel substrate

The influence of the concentration of DMH, citrate, and K_2CO_3 and the value of pH on the adhesion of copper layers electrodeposited on carbon steel substrate was investigated with three qualitative methods and the results are listed in Table 5. The copper layers obtained from solutions

without DMH did not pass the bend test. This may result from the immersion coating of copper on steel substrate, as the citrate concentration was too low to prevent the contact replacement reaction by coordinating with cupric ion. The adhesion was good in the investigated range (0.1 to 0.5 M) of the citrate concentration. In the solution with high concentration of K_2CO_3 (0.5 M), the adhesion was also not good enough to pass the bend test, which may be ascribed to the strong hydrogen evolution as demonstrated in Figure 13 (6) [42, 43]. The copper layers obtained at pH 8.5 detached from the substrate at bend test because copper ions also could not coordinate with DMH and citrate very well at low pH condition. In addition, the cross-sectional SEM image of the copper layer electroplated from S2 at 15 mA/cm^2 is given in Figure 15 (see more in Figure S12 of supplementary materials). No slit can be observed at the joint area, which further confirms the good adhesion of copper layer on the carbon steel substrate.

Table 5 the adhesion of the copper layers electrodeposited from various solutions

DMH (M)		Citrate (M)		K_2CO_3 (M)		pH	
0.0	no	0.1	yes	0.1	yes	8.5	no
0.2	yes	0.3	yes	0.3	yes	9	yes
0.4	yes	0.5	yes	0.5	no	10.5	yes

4 Conclusions

We have use cyclic voltammetry, chronoamperometry, chronopotentiometry, and cathodic polarization to study the electrodeposition of copper in solution with only DMH, only citrate, and both as the complex agents. Molecular dynamic simulation reveals the adsorption behaviour and interaction energy of DMH, citrate acid, and HCN molecules on Cu (111) and Fe (111) surface. Copper layers were characterized by SEM for surface morphology, XRD for crystal structure, and three qualitative methods for adhesion evaluation.

Cyclic voltammetry study at various switch potentials and at various scan rates shows that the discharge process on the Pt or GC electrode in the solutions with only DMH, only citrate, and both as the complex agents has two steps and is irreversible. Kinetic parameters are obtained easily from the sample current voltammograms with the results in correspondence to the ones from cyclic voltammetry. The different transfer coefficients α obtained from the Pt and GC electrode in solution with only DMH as the complex agent indicates different discharge mechanism, which is also revealed by cyclic voltammetry as cyclic voltammograms of the two systems have two different shapes.

The analysis of chronoamperometry on the Pt and GC electrode in solution with only DMH as the complex agent gives two almost identical results, 3.54×10^{-7} and 3.61×10^{-7} $cm^2 \cdot s^{-1}$. At the same time, the theoretic current density *vs*. time curves with the fitted results based on the Contrell equation match very well with the experimental curves. All the three systems with only DMH, only citrate, and both as the complex agents have the progressive nucleation process of SH, according to the comparison of the experimental curves to the dimensionless theoretical curves. Moreover, DMH have a stronger influence on the nucleation and crystal growth process of copper on the GC electrode in solution Sp3 with both DMH and citrate as the complex agents in the experimental composition.

Additionally, DMH molecules adsorb on the Fe (111) surface with the plane of the heterocycle parallel to the Fe (111) surface revealed by molecular dynamic simulation. DMH and citrate acid, no matter with or without negative charge, adsorb stronger on Fe (111) than on Cu (111). DMH molecules show larger interaction energy than citrate acid molecule on both Fe (111) and Cu (111). Chronopotentiometry study shows that DMH molecules adsorbed on carbon steel electrode desorb

at the initial stage of electrodeposition. These confirm that DMH act not only as the complex agent, but also the inhibiters by adsorbing on the substrate surface, which can prevent the passivation of the steel substrate.

The concentration of DMH and K_2CO_3 and the value of pH have a crucial effect on the adhesion, the morphology, and preferable crystal orientation of the copper layers electroplated on carbon steel substrate. The baths have a current efficiency more than 80% at 10 mA/cm^2 according to the deposition/stripping method based on constant−current chronopotentiometry.

Finally, the optimum bath composition and conditions for copper electroplating on carbon steel substrate are as follows: 0.1 M $CuSO_4$, 0.2 M DMH, 0.3 M citrate, and 0.3 M K_2CO_3, pH = 9 ~ 10, at 50℃, current density range from 5 to 25 mA/cm^2, and with strong agitation. Copper layers with average grain size of around 30 nm and good adhesion can be electroplated on carbon steel substrate from the baths. As the study in this paper almost focuses on the electrodeposition mechanism, more work about specific technologies and applications is needed in the further study. We suggest the following studies: longer-term deposition, thicker deposit, and bath ageing studies, Hull cell studies to determine acceptable electroplating ranges of current density for various operating conditions and bath compositions, controlled hydrodynamic studies using rotating disc and cylinder electrodes, and Haring-Blum throwing power studies.

Acknowledgements

The authors are grateful for financial support from the State Key Laboratory of Urban Water Resource and Environment (Harbin Institute of Technology) (2012DX03).

References

1. F. A. Lowenheim, *Modern Electroplating,5th*, J. Wiley & Sons, New York, USA, 2010.
2. Z. A. Hamid and A. A. Aal, *Surface & Coatings Technology*, 2009, 203, 1360-1365.

3. L. L. Barbosa, M. R. H. de Almeida, R. M. Carlos, M. Yonashiro, G. M. Oliveira and I. A. Carlos, *Surface & Coatings Technology*, 2005, 192, 145-153.

4. C. N. Tharamani, B. N. Maruthi and S. M. Mayanna, *Transactions of the Institute of Metal Finishing*, 2002, 80, 37-39.

5. J. C. Ballesteros, E. Chainet, P. Ozil, Y. Meas and G. Trejo, *International Journal of Electrochemical Science*, 2011, 6, 1597-1616.

6. J. C. Ballesteros, E. Chainet, P. Ozil, G. Trejo and Y. Meas, *Journal of Electroanalytical Chemistry*, 2010, 645, 94-102.

7. Y. Xiaowei, A. Maozhong, Z. Yunwang and Z. Lin, *Electrochimica Acta*, 2011, 58, 516-522.

8. A. M. Liu, X. F. Ren, M. Z. An, J. Q. Zhang, P. X. Yang, B. Wang, Y. M. Zhu and C. Wang, *Scientific Reports*, 2014, 4.

9. *US Pat.,* US20110180415 A1, 2011.

10. *US Pat.,* US5750018 A, 1998.

11. A. Gerasimenko, M. Kirvoruchko and V. Korzhavina, *Protection of Metals*, 2000, 6, 1597-1616.

12. N. Kanani, *Electroplating: Basic Principles, Processes and Practice*, Elsevier Science, 2004.

13. S. B. Feng, S. B. Shang, X. Bao, L. T. Feng, J. W. Zhang and Z. H. Li, *Acta Phys.-Chim. Sin.*, 2005, 21, 463-467.

14. G. Z. Pavlovich and R. G. Luthy, *Water Research*, 1988, 22, 327-336.

15. K. Oyaizu, Y. Ohtani, A. Shiozawa, K. Sugawara, T. Saito and M. Yuasa, *Inorganic Chemistry*, 2005, 44, 6915-6917.

16. R. W. Revie, *Corrosion and Corrosion Control*, Wiley, 2008.

17. L. H. Madkour, A. M. Hassanein, M. M. Ghoneim and S. A. Eid, *Monatshefte fuer Chemie*, 2001, 132, 245-258.

18. A. O. Yüce and G. Kardaş, *Corrosion Science*, 2012, 58, 86-94.

19. C. Wang, M. An, P. Yang and J. Zhang, *Electrochemistry Communications*, 2012, 18, 104-107.

20. S. Monti, C. Li and V. Carravetta, *Journal of Physical Chemistry C*, 2013, 117, 5221-5228.

21. F. I. Lizama-Tzec, L. Canché-Canul and G. Oskam, *Electrochimica Acta*, 2011, 56, 9391-9396.

22. S. Rode, C. Henninot, C. C. Vallieres and M. Matlosz, *Journal of the Electrochemical Society*, 2004, 151, C405-C411.

23. T. A. Green, A. E. Russell and S. Roy, *Journal of the Electrochemical Society*, 1998, 145, 875-881.

24. E. Beltowska-Lehman and P. Ozga, *Electrochimica Acta*, 1998, 43, 617-629.

25. *US Pat.,* US4595462 A, 1986.

26. P. Bos and E. V. Dalen, *Journal of Electroanalytical Chemistry and Interfacial Electrochemistry*, 1968, 17, 21-30.

27. A. Plankova, K. M. Matar, P. Rauko and L. Novotny, *Journal of Pharmacy and Pharmaceutical Sciences*, 2010, 13, 391-399.

28. M. V. Mirkin and A. J. Bard, *Anal Chem*, 1992, 64, 2293-2302.

29. B. Scharifker and G. Hills, *Electrochimica Acta*, 1983, 28, 879-889.

30. M. E. Hyde and R. G. Compton, *Journal of Electroanalytical Chemistry*, 2003, 549, 1-12.

31. R. Drissi-Daoudi, A. Irhzo and A. Darchen, *Journal of Applied Electrochemistry*, 2003, 33, 339-343.

32. A. Ramos, M. Miranda-Hernandez and I. Gonzalez, *Journal of the Electrochemical Society*, 2001, 148, C315-C321.

33. R. Y. Ying, P. K. Ng, Z. Mao and R. E. White, *Journal of The Electrochemical Society*, 1988, 135, 2964-2971.

34. A. J. Bard and L. R. Faulkner, *Electrochemical Methods: Fundamentals and Applications*, Wiley, 2000.

35. H. A. Laitinen and I. M. Kolthoff, *Journal of the American Chemical Society*, 1939, 61, 3344-3349.

36. D. Grujicic and B. Pesic, *Electrochimica Acta*, 2002, 47, 2901-2912.

37. S. Floate, M. Hyde and R. G. Compton, *Journal of Electroanalytical Chemistry*, 2002, 523, 49-63.

38. K. Ogura and H. Wada, *Electrochimica Acta*, 1980, 25, 913-917.

39. A. J. Davenport, J. A. Bardwell and C. M. Vitus, *Journal of the Electrochemical Society*, 1995, 142, 721-724.

40. S. Ghosh and S. Roy, *Surface and Coatings Technology*, 2014, 238, 165-173.

41. A. Ibañez and E. Fatás, *Surface and Coatings Technology*, 2005, 191, 7-16.

42. J. Gui and T. M. Devine, *Corrosion Science*, 1995, 37, 1177-1189.

43. J. Banaś, U. Lelek-Borkowska, B. Mazurkiewicz and W. Solarski, *Electrochimica Acta*, 2007, 52, 5704-5714.

List of figure captions:

Figure 1. Cyclic voltammograms of the Pt electrode in solution Sp4 with only DMH as the complex agent. (a) In the range from 1.0 V to −1.5 V *vs*. SCE and (b) In the range from 1.0 V to various switch potentials *vs*. SCE. The scan rate is 50 mV/s. The blue dash line signed by "Empty with DMH" in (a) was obtained from the background solution composed with 0.2 M DMH and 0.3 M K_2CO_3 at pH = 9 and 50℃.

Figure 2. Cyclic voltammograms of the GC electrode in solution Sp4 with only DMH as the complex agent. (a) In the range from 1.0 V to −1.5 V *vs*. SCE and (b) In the range from 1.0 V to various switch potentials *vs*. SCE. The scan rate is 50 mV/s.

Figure 3. Cyclic voltammograms of the GC electrode in solution Sp1 with only citrate as the complex agent. (a) In the range from 1.0 V to −1.5 V *vs*. SCE and (b) In the range from 1.0 V to various switch potentials *vs*. SCE. The scan rate is 50 mV/s.

Figure 4. Cyclic voltammograms of the GC electrode in solution Sp3 with both DMH and citrate as the complex agents in the range from 1.0 V to −1.25 V and −1.5 V *vs*. SCE. The scan rate is 50 mV/s.

Figure 5. Cyclic voltammograms at various scan rates. (a) The Pt electrode in solution Sp4 with only DMH as the complex agent, (b) The GC electrode in solution Sp4 with only DMH as the complex agent, (c) The GC electrode in solution Sp1 with only citrate as the complex agent, (d) The GC electrode in solution Sp3 with both DMH and citrate as the complex agents. The insets are j_p *vs*. $v^{1/2}$ lines fitted from the peak of cathodic current density at various scan rates.

Figure 6. (a) The sample current voltammogram of the Pt electrode in the solution Sp4 with only DMH as the complex agent. (b) The E *vs*. lnj curves fitted from the data of the sample current voltammetry. .

Figure 7. The j *vs*. $t^{1/2}$ line fitted according Contrell equation from the j *vs*. time curves obtained from solution Sp4 with only DMH as the complex agent. (a) On the Pt electrode and (b) On the GC electrode with the potential changed from 0.2 V to −0.16 *vs*. SCE.

Figure 8. The chronoamperometry at various step potentials and the corresponding dimensionless experimental curves with their theoretical curves for instantaneous and progressive nucleation processes of the GC electrode in different solutions. (a) and (A) In solution Sp4 with only DMH as the complex agent, (b) and (B) In solution Sp1 with only citrate as the complex agent, (c) and (C) In solution Sp3 with both DMH and citrate as the complex agents.

Figure 9. The front and top views of the simulated behaviors of DMH on Cu (111) (A and a) and Fe (111) (B and b) surfaces.

Figure 10. Potential *vs*. time curves of a carbon steel electrode as a function of step−current in S2 and cupric ions free solutions. Curve (a) was obtained from the background solution consisting of 0.3 M citrate, and 0.3 M K_2CO_3. Curve (b) from the background solution consisting of 0.2 M DMH, 0.3 M

citrate, and 0.3 M K_2CO_3. All solutions were at pH 9 and 50℃.

Figure 11. Cathodic polarization curves as a function of (a) citrate, (b) DMH, (c) pH, and (d) temperature with the Pt RDE as the work electrode at 300 rpm and scan rate of 1 mV/s. (a) and (b) were obtained from S1, S2, S3, S4, S5 at pH 9 and 50℃, (c) at various pH from solution S2 at 50℃, and (d) at various temperatures from solution S2 at pH 9.

Figure 12. CE as a function of current density at various solutions and conditions with pH 9. (a) S2 at 50℃, (b) S2 at 40℃, (c) 0.1 M Cu2+, 0.4 M DMH, and 0.3 M K_2CO_3 at 50℃ and pH 9.

Figure 13. SEM images illustrating the morphology of copper layers electrodeposited from various solutions at pH 9 and 50℃: (1) S1, (2) S2, (3) S4, (4) S5, (5) S6, and (6) S7, and from S2 with various pH at 50℃: (7) pH 8.5, and (8) pH 10.5.

Figure 14. XRD patterns of the copper layers corresponding to the images in figure S11. The copper layers were electroplated from various solutions at pH 9 and 50℃: (1) S1, (2) (5) and (8) S2, (3) S3, (4) S4, (6) S5, (7) S6, and (9) S7, and from S2 with various pH at 50℃: (10) pH 8.5, (11) pH 9, and (12) pH 10.5.

Figure 15. Cross-sectional SEM image of the copper layer electrodeposited from S2 at 15 mA/cm^2 for 30 min.

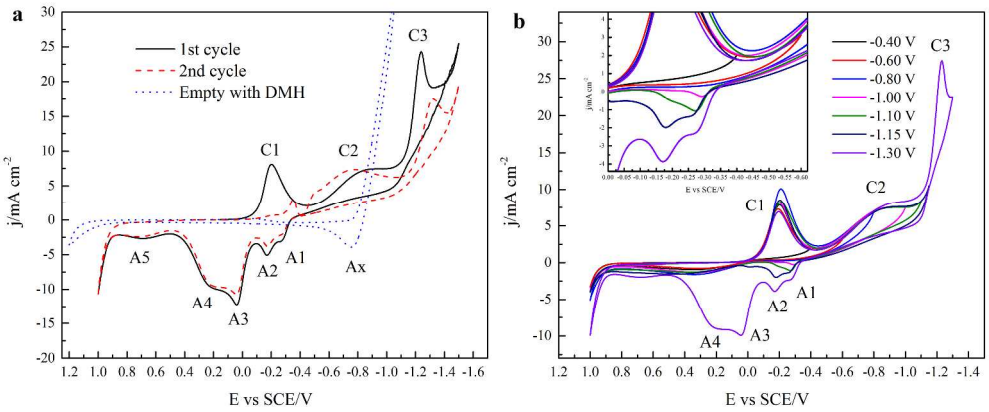

1868x784mm (72 x 72 DPI)

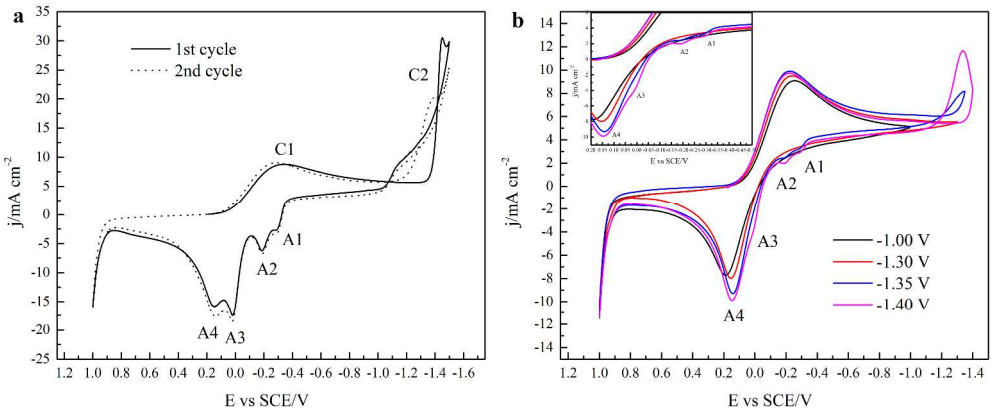

1854x782mm (72 x 72 DPI)

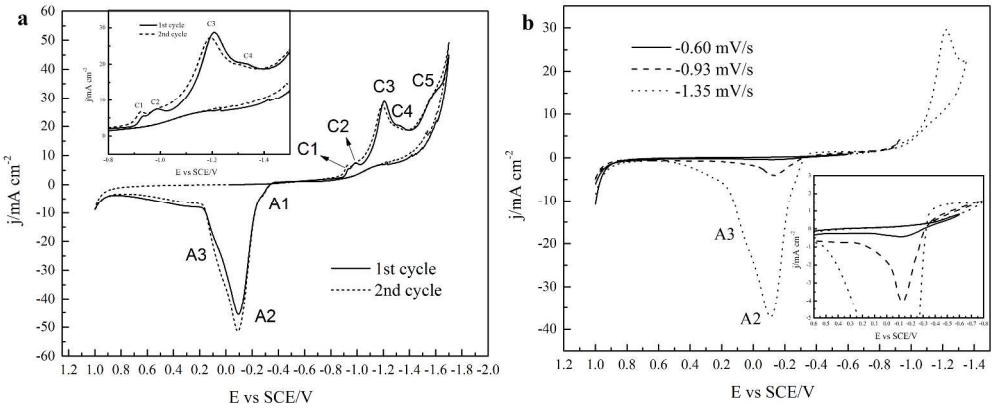

1865x767mm (72 x 72 DPI)

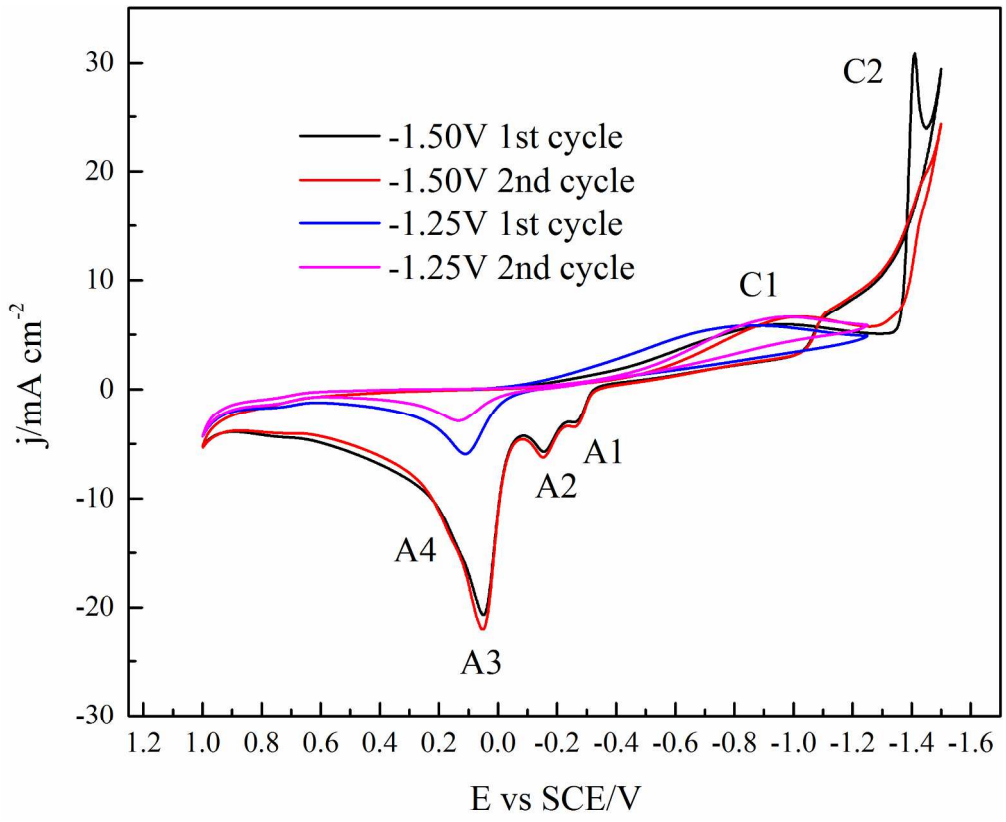

218x178mm (300 x 300 DPI)

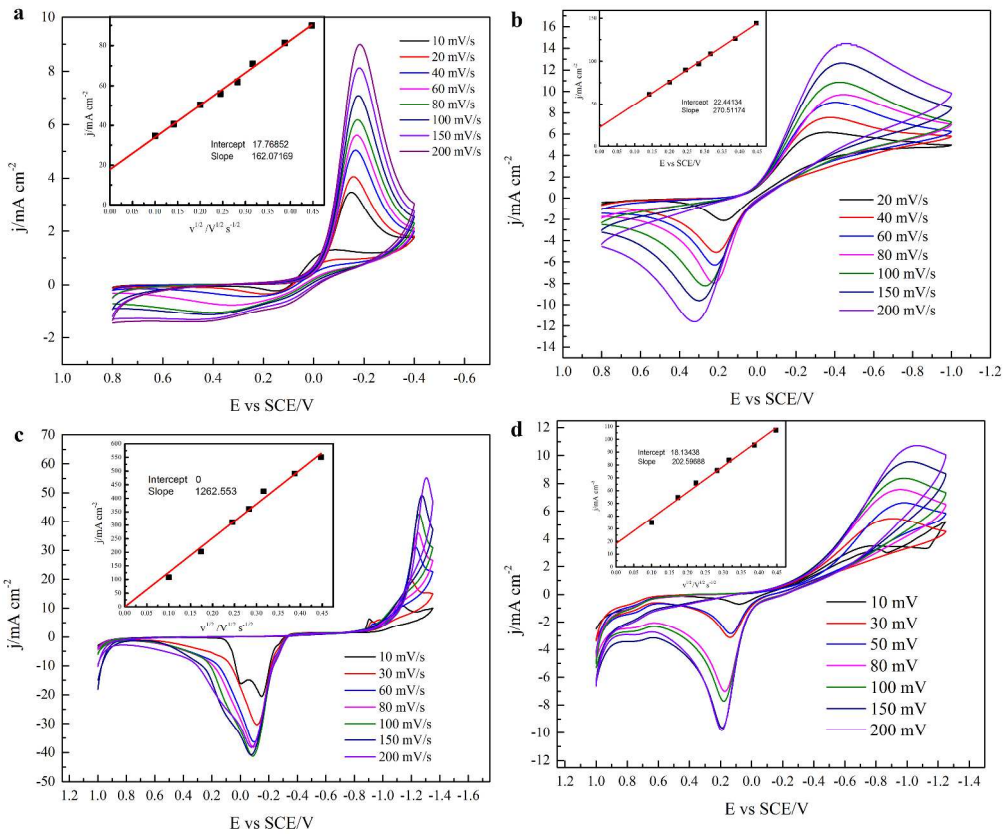

1860x1546mm (72 x 72 DPI)

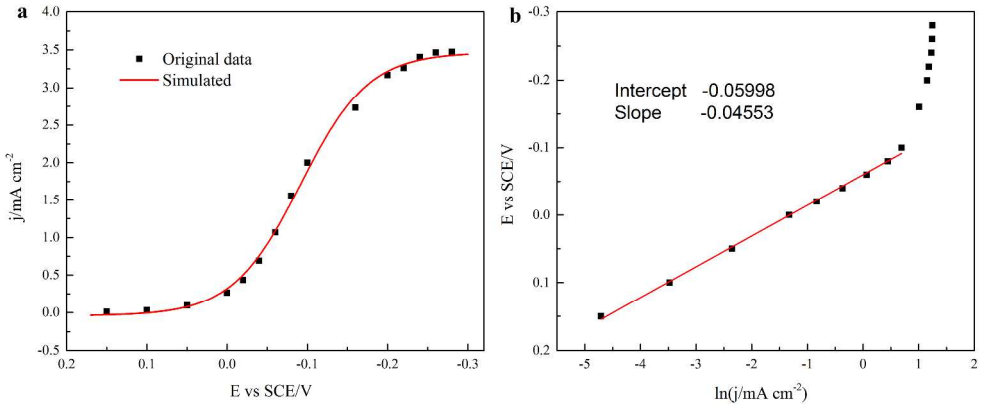

1905x778mm (72 x 72 DPI)

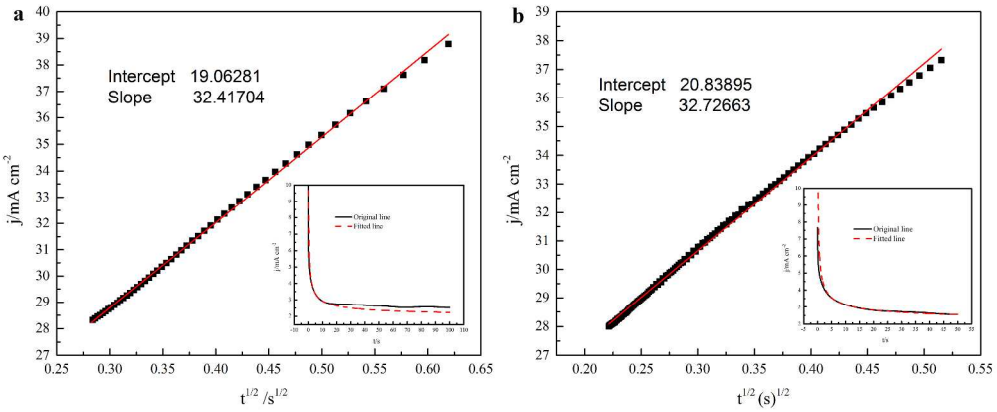

1871x779mm (72 x 72 DPI)

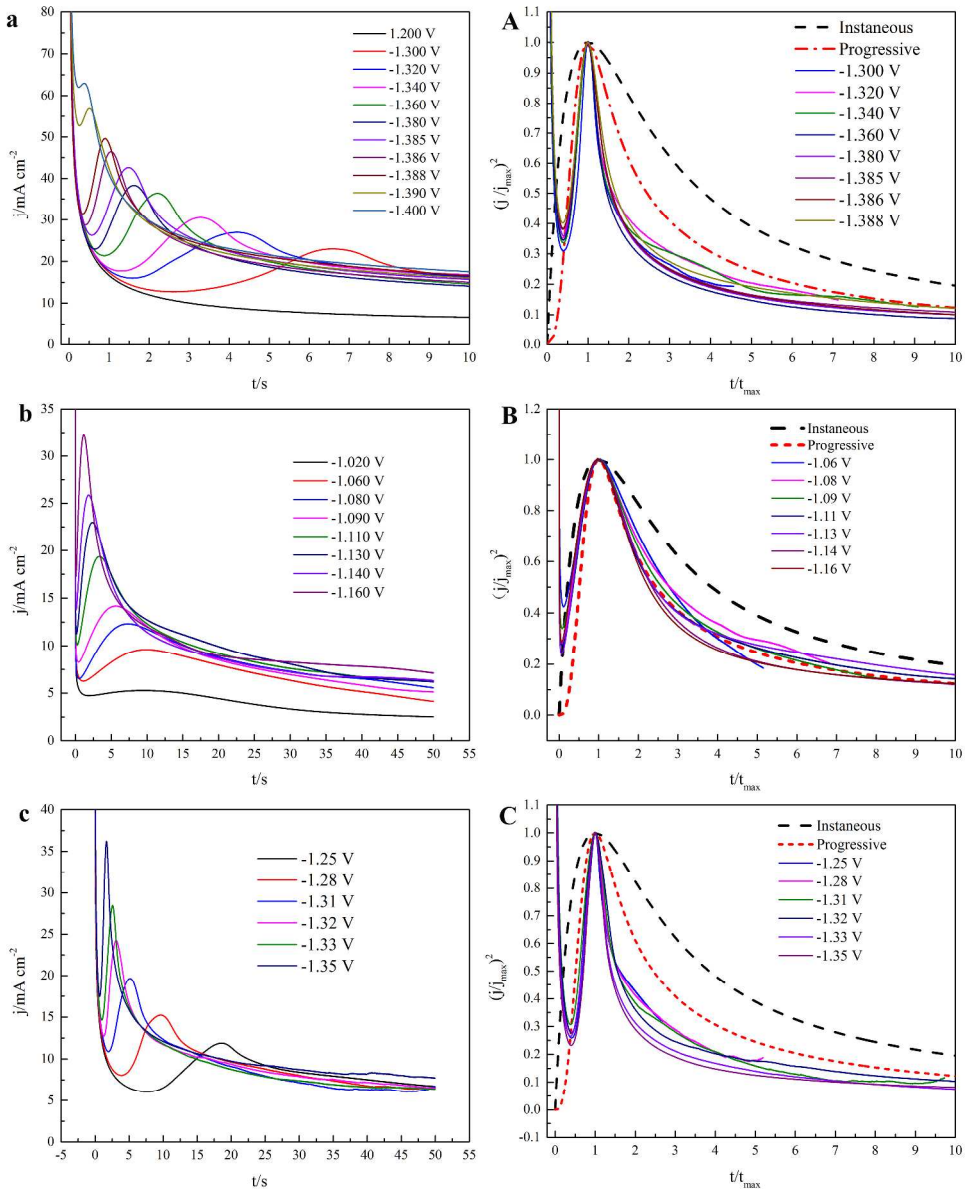

1896x2334mm (72 x 72 DPI)

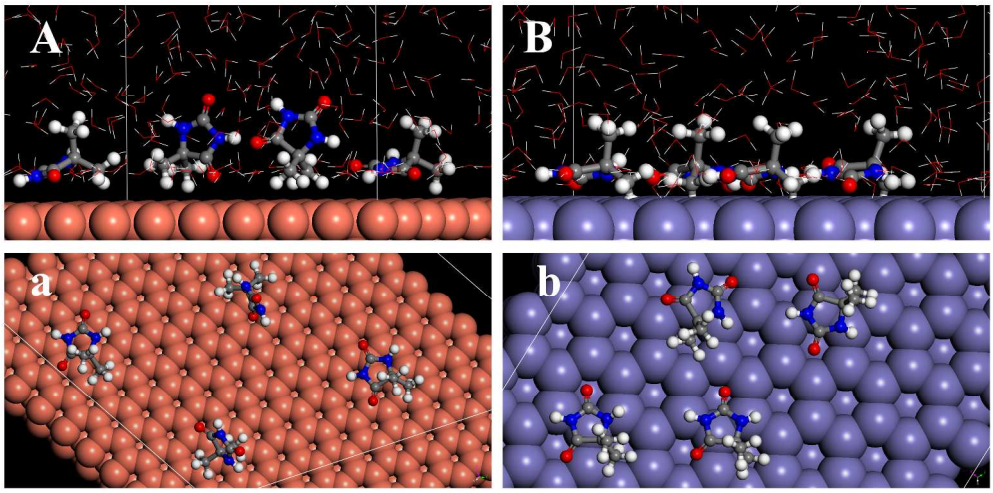

1143x570mm (72 x 72 DPI)

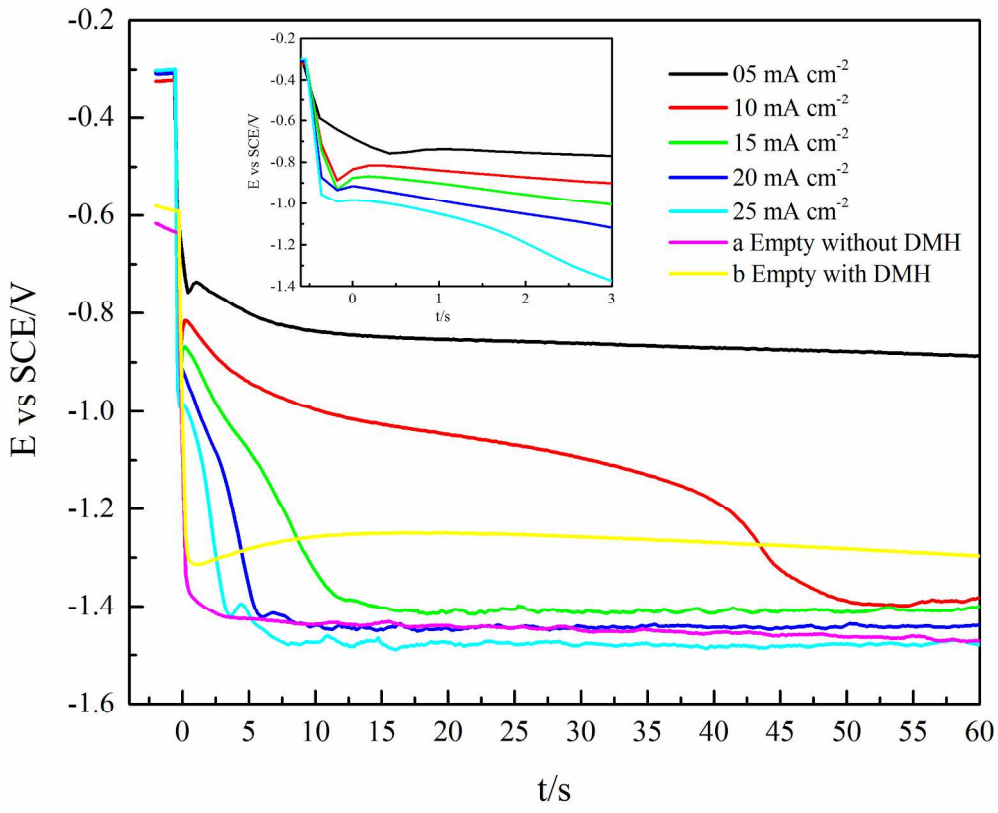

213x173mm (300 x 300 DPI)

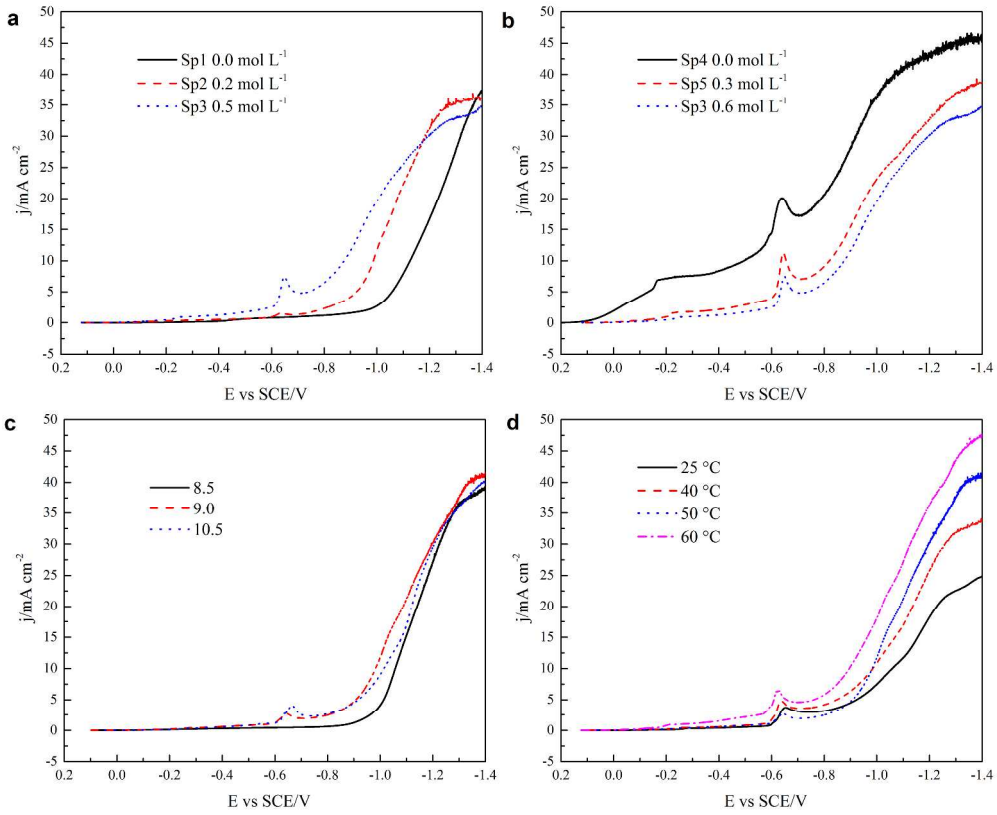

1888x1541mm (72 x 72 DPI)

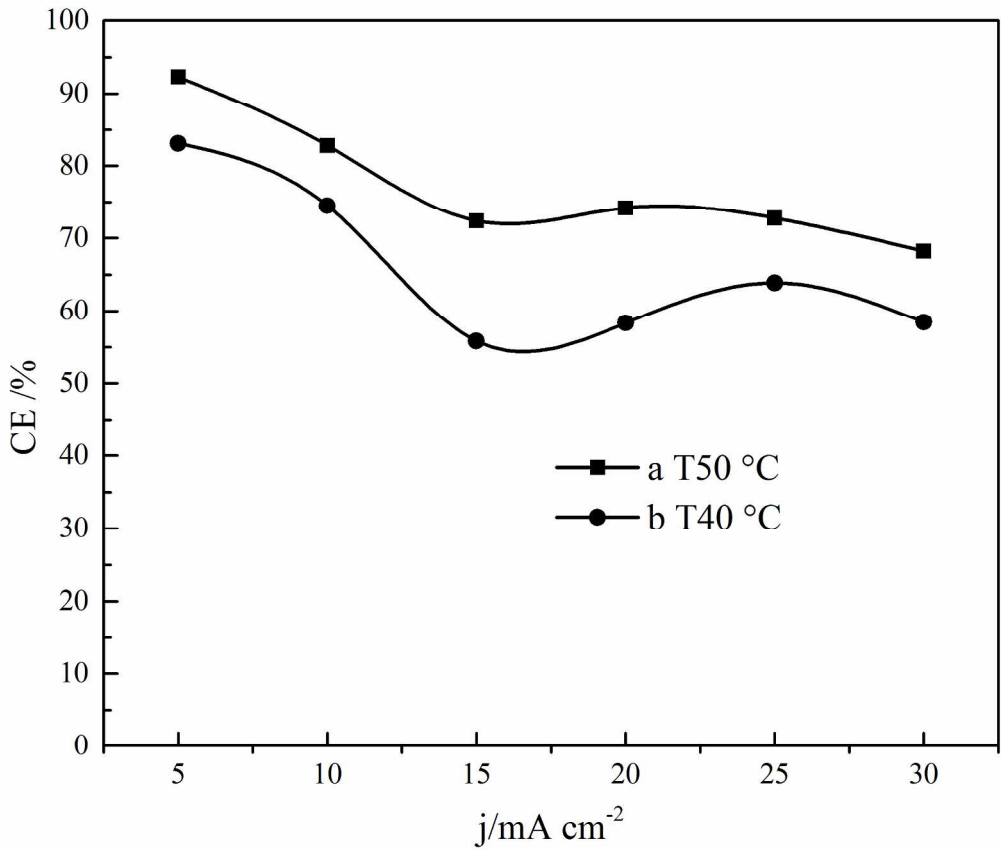

213x182mm (300 x 300 DPI)

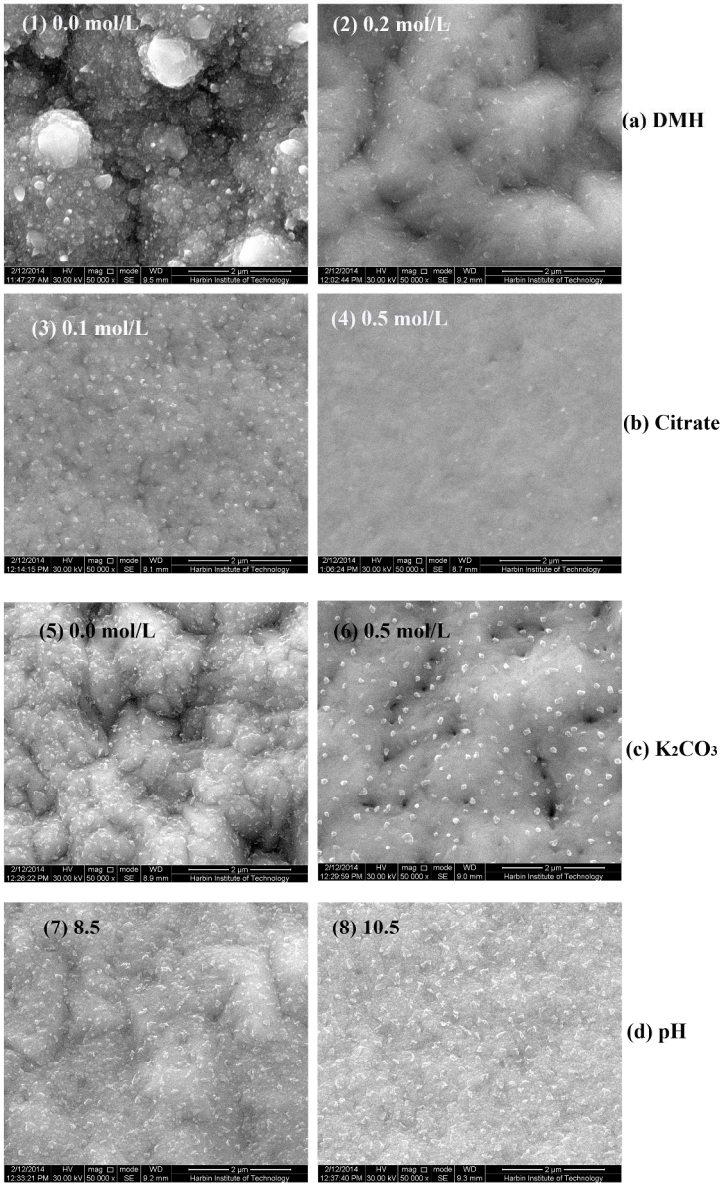

878x1425mm (72 x 72 DPI)

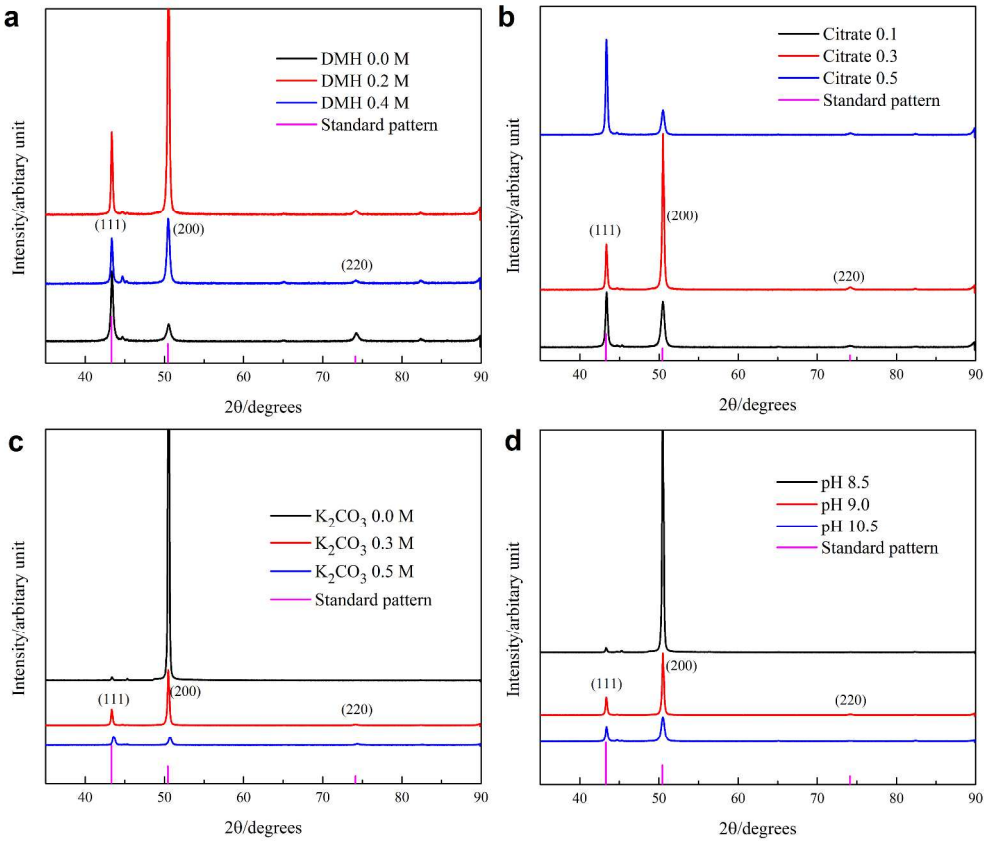

1826x1532mm (72 x 72 DPI)

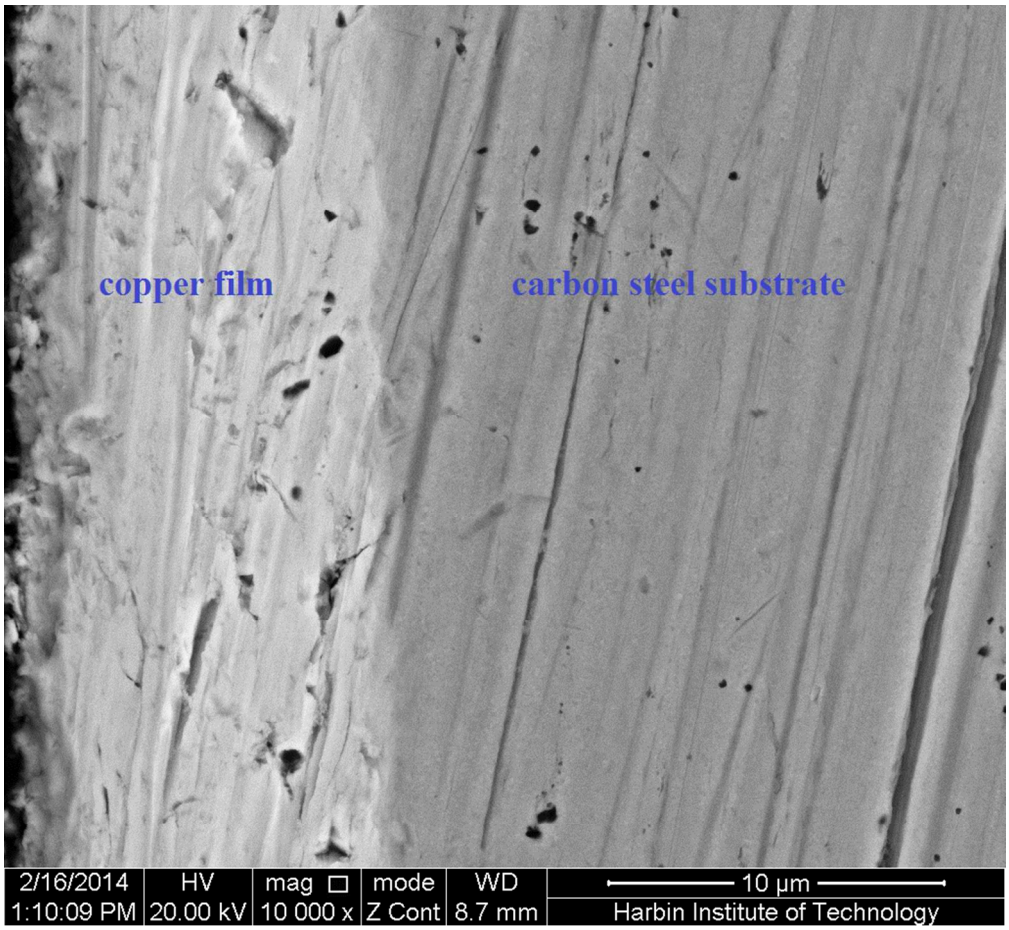

302x278mm (86 x 86 DPI)